New More Efficient A-WENO Schemes

Shaoshuai Chu[*], Alexander Kurganov[†], and Ruixiao Xin[‡]

Abstract

We develop new more efficient A-WENO schemes for both hyperbolic systems of conservation laws and nonconservative hyperbolic systems. The new schemes are very simple modification of the existing A-WENO schemes: They are obtained by a more efficient evaluation of the high-order correction terms. We conduct several numerical experiments to demonstrate the performance of the introduced schemes.

Key words: Finite-difference schemes, A-WENO schemes, flux globalization based well-balanced path-conservative A-WENO schemes, finite-volume numerical fluxes, high-order correction terms.

AMS subject classification: 76M12, 65M08, 76N15, 35L65, 35L67.

1 Introduction

This paper is focused on the development of new more efficient fifth-order finite-difference (FD) alternative weighted essentially non-oscillatory scheme (A-WENO) schemes for both conservative and nonconservative hyperbolic systems of nonlinear PDEs.

In the one-dimensional (1-D) case, hyperbolic systems of conservation laws read as

$$\boldsymbol{U}_t+\boldsymbol{F}(\boldsymbol{U})_x=\boldsymbol{0}, \tag{1.1}$$

where x is the spatial variable, t is the time, $\boldsymbol{U}\in\mathbb{R}^d$ is a vector of unknowns, $\boldsymbol{F}:\mathbb{R}^d\to\mathbb{R}^d$ is a nonlinear flux function. The A-WENO schemes for (1.1), introduced in [23] (also see [11, 14, 18, 31, 32, 40–42]), employ finite-volume (FV) numerical fluxes without any flux splitting, and use high-order correction terms to ensure a high-order spatial accuracy of the resulting scheme. For instance, the original A-WENO scheme from [23] employs an upwind flux, the schemes in [18, 31, 32, 40, 42] rely on the simplest—yet very robust—central (local Lax-Friedrichs, Rusanov) flux or its adaptive version, and the schemes in [11, 14, 41] are based on central-upwind fluxes. Examples of many other FV numerical fluxes can be found in, e.g., [22, 24, 30, 39].

In this paper, we focus on the computation of the high-order correction terms. In all of the existing A-WENO schemes, these terms are computed using the point values of the flux function

[*]Department of Mathematics and Shenzhen International Center for Mathematics, Southern University of Science and Technology, Shenzhen, 518055, China; chuss@mail.sustech.edu.cn

[†]Department of Mathematics, Shenzhen International Center for Mathematics, and Guangdong Provincial Key Laboratory of Computational Science and Material Design, Southern University of Science and Technology, Shenzhen, 518055, China; alexander@sustech.edu.cn

[‡]Department of Mathematics, Southern University of Science and Technology, Shenzhen, 518055, China; 12331009@mail.sustech.edu.cn

$\boldsymbol{F}(\boldsymbol{U})$. This requires the fluxes to be evaluated at every grid point at every time step. We propose to use the already computed numerical fluxes instead of evaluating the flux function at the grid points: This way one can save the computational time without losing accuracy or risking any additional spurious oscillations.

The proposed modification can also be applied to the nonconservative hyperbolic systems, which in the 1-D case read as

$$\boldsymbol{U}_t + \boldsymbol{F}(\boldsymbol{U})_x = B(\boldsymbol{U})\boldsymbol{U}_x, \tag{1.2}$$

where $B(\boldsymbol{U}) \in \mathbb{R}^{d\times d}$. The presence of the nonconservative products on the right-hand side (RHS) of (1.2) introduces more challenges for studying (1.2) both theoretically and numerically. Weak solutions of (1.2) can be understood in the sense of Borel measures as it was done in [16, 28, 29], but not in the sense of distributions when $\boldsymbol{U}$ is discontinuous. The concept of Borel measure solutions was utilized to develop path-conservative schemes. A wide of variety of path-conservative methods have been introduced; see, e.g. [2–4,6–9,26,34,35,37] and references therein. Recently, the second-order path-conservative central-upwind scheme from [8] has been extended to fifth order of accuracy in the framework of A-WENO schemes; see, e.g., [12, 13]. In these schemes, we first rewrite the system (1.2) in the following quasi-conservative form:

$$\boldsymbol{U}_t + \boldsymbol{K}(\boldsymbol{U})_x = \boldsymbol{0}, \tag{1.3}$$

where

$$\boldsymbol{K}(\boldsymbol{U}) = \boldsymbol{F}(\boldsymbol{U}) - \boldsymbol{R}(\boldsymbol{U}), \quad \boldsymbol{R}(\boldsymbol{U}) := \int\limits_{\widehat{x}}^{x} B(\boldsymbol{U})\boldsymbol{U}_\xi(\xi,t)\,\mathrm{d}\xi,$$

and $\widehat{x}$ is an arbitrary number. High-order correction terms are then computed using the point values of the global fluxes $\boldsymbol{K}$. As in the conservative case, the point values of $\boldsymbol{K}$ need to be computed at every grid point at every time step. In this paper, we propose a more efficient alternative: to use the already computed numerical flux values in the computation of the high-order correction terms, which leads to new more efficient A-WENO schemes for nonconservative hyperbolic systems. The proposed A-WENO schemes are realized in the framework of flux globalization based well-balanced (WB) path-conservative schemes, which were introduced in [26] and later applied to a variety of shallow water models in [3, 4, 10].

The rest of the paper is organized as follows. In §2.1, we briefly describe the existing A-WENO schemes and then in §2.2, we introduce new A-WENO schemes using an alternative, more efficient way of computing the high-order correction terms. In §3.1, we describe flux globalization based WB path-conservative A-WENO schemes, and then introduce new more efficient flux globalization based WB path-conservative A-WENO schemes in §3.2. Finally, in §4, we test the proposed schemes on a number of conservative and nonconservative examples. The obtained numerical results demonstrate that the new A-WENO schemes are clearly more efficient than the old ones, while neither the accuracy nor the quality of resolution is affected by switching to the new approach.

2 Fifth-Order A-WENO Schemes for (1.1)

2.1 Existing A-WENO Schemes

We assume that the computational domain is covered with uniform cells $C_j := [x_{j-\frac12}, x_{j+\frac12}]$ of size $x_{j+\frac12} - x_{j-\frac12} \equiv \Delta x$ centered at $x_j = (x_{j-\frac12} + x_{j+\frac12})/2$, $j = 1, \ldots, N_x$. We also assume that at a certain time $t \geq 0$, the point values of the computed solution, $\boldsymbol{U}_j(t)$, are available (in the rest of the paper, we will suppress the time-dependence of all of the indexed quantities for the sake of brevity). In the framework of semi-discrete A-WENO schemes, $\boldsymbol{U}_j$ are evolved in time by solving the following system of ODEs:

$$\frac{\mathrm{d}\boldsymbol{U}_j}{\mathrm{d}t} = -\frac{\boldsymbol{\mathcal{F}}_{j+\frac12} - \boldsymbol{\mathcal{F}}_{j-\frac12}}{\Delta x}, \tag{2.1}$$

where $\boldsymbol{\mathcal{F}}_{j+\frac12}$ are the fifth-order numerical fluxes, computed by

$$\boldsymbol{\mathcal{F}}_{j+\frac12} = \boldsymbol{\mathcal{F}}^{\rm FV}_{j+\frac12} - \frac{(\Delta x)^2}{24}(\boldsymbol{F}_{xx})_{j+\frac12} + \frac{7(\Delta x)^4}{5760}(\boldsymbol{F}_{xxxx})_{j+\frac12}. \tag{2.2}$$

Here, $\boldsymbol{\mathcal{F}}^{\rm FV}_{j+\frac12} = \boldsymbol{\mathcal{F}}^{\rm FV}_{j+\frac12}\big(\boldsymbol{U}^-_{j+\frac12}, \boldsymbol{U}^+_{j+\frac12}\big)$ stand for FV numerical fluxes, which depends on $\boldsymbol{U}^-_{j+\frac12}$ and $\boldsymbol{U}^+_{j+\frac12}$, which are the left- and right-sided values of $\boldsymbol{U}$ at $x = x_{j+\frac12}$ computed using the WENO-Z interpolation procedure introduced in [1,5,17]. In this paper, we have utilized one of the simplest FV numerical fluxes—the central (local Lax-Friedrichs, Rusanov) fluxes (see [27,36]):

$$\boldsymbol{\mathcal{F}}^{\rm FV}_{j+\frac12} = \frac{\boldsymbol{F}(\boldsymbol{U}^-_{j+\frac12}) + \boldsymbol{F}(\boldsymbol{U}^+_{j+\frac12})}{2} - \frac{a_{j+\frac12}}{2}\big(\boldsymbol{U}^+_{j+\frac12} - \boldsymbol{U}^-_{j+\frac12}\big),$$

where the local speed of propagation $a_{j+\frac12}$ is estimated using the eigenvalues $\lambda_1(A) \leq \ldots \leq \lambda_d(A)$ of the Jacobian $A = \frac{\partial \boldsymbol{F}}{\partial \boldsymbol{U}}$:

$$a_{j+\frac12} = \max_j \Big\{\big|\lambda_1\big(A(\boldsymbol{U}^-_{j+\frac12})\big)\big|, \big|\lambda_1\big(A(\boldsymbol{U}^+_{j+\frac12})\big)\big|, \big|\lambda_d\big(A(\boldsymbol{U}^-_{j+\frac12})\big)\big|, \big|\lambda_d\big(A(\boldsymbol{U}^+_{j+\frac12})\big)\big|\Big\}.$$

Finally, the higher-order correction terms $(\boldsymbol{F}_{xx})_{j+\frac12}$ and $(\boldsymbol{F}_{xxxx})_{j+\frac12}$ are the second- and fourth-order spatial numerical derivatives of $\boldsymbol{F}$ at the cell interface $x = x_{j+\frac12}$, which are computed using the following FD approximations:

$$\begin{aligned}
(\boldsymbol{F}_{xx})_{j+\frac12} &= \frac{1}{48(\Delta x)^2}\left(-5\boldsymbol{F}_{j-2} + 39\boldsymbol{F}_{j-1} - 34\boldsymbol{F}_j - 34\boldsymbol{F}_{j+1} + 39\boldsymbol{F}_{j+2} - 5\boldsymbol{F}_{j+3}\right),\\
(\boldsymbol{F}_{xxxx})_{j+\frac12} &= \frac{1}{2(\Delta x)^4}\left(\boldsymbol{F}_{j-2} - 3\boldsymbol{F}_{j-1} + 2\boldsymbol{F}_j + 2\boldsymbol{F}_{j+1} - 3\boldsymbol{F}_{j+2} + \boldsymbol{F}_{j+3}\right),
\end{aligned} \tag{2.3}$$

where $\boldsymbol{F}_j := \boldsymbol{F}(\boldsymbol{U}_j)$.

2.2 New A-WENO Schemes

In this section, we provide an alternative, more efficient way of computing the high-order correction terms $(\boldsymbol{F}_{xx})_{j+\frac12}$ and $(\boldsymbol{F}_{xxxx})_{j+\frac12}$, which are obtained by

$$\begin{aligned}
(\boldsymbol{F}_{xx})_{j+\frac12} &= \frac{1}{12(\Delta x)^2}\Big[-\boldsymbol{\mathcal{F}}^{\rm FV}_{j-\frac32} + 16\boldsymbol{\mathcal{F}}^{\rm FV}_{j-\frac12} - 30\boldsymbol{\mathcal{F}}^{\rm FV}_{j+\frac12} + 16\boldsymbol{\mathcal{F}}^{\rm FV}_{j+\frac32} - \boldsymbol{\mathcal{F}}^{\rm FV}_{j+\frac52}\Big],\\
(\boldsymbol{F}_{xxxx})_{j+\frac12} &= \frac{1}{(\Delta x)^4}\Big[\boldsymbol{\mathcal{F}}^{\rm FV}_{j-\frac32} - 4\boldsymbol{\mathcal{F}}^{\rm FV}_{j-\frac12} + 6\boldsymbol{\mathcal{F}}^{\rm FV}_{j+\frac12} - 4\boldsymbol{\mathcal{F}}^{\rm FV}_{j+\frac32} + \boldsymbol{\mathcal{F}}^{\rm FV}_{j+\frac52}\Big].
\end{aligned} \tag{2.4}$$

Notice that the main difference between (2.4) and (2.3) is that in (2.4), we use FD approximations of $(\boldsymbol{F}_{xx})_{j+\frac12}$ and $(\boldsymbol{F}_{xxxx})_{j+\frac12}$ terms with the help of the FV numerical fluxes $\boldsymbol{\mathcal{F}}^{\rm FV}_{j+\frac12}$ instead of the point values $\boldsymbol{F}_j$. Clearly, the new A-WENO schemes are less computationally expensive than the original ones as they do not require computing the point values $\boldsymbol{F}_j$, while the values $\boldsymbol{\mathcal{F}}^{\rm FV}_{j+\frac12}$ have to be computed in (2.2) and then can be stored. At the same time, the new A-WENO schemes are still fifth-order accurate and they can achieve the same high resolution as the original A-WENO schemes as demonstrated in §4, where we present several numerical examples.

Remark 2.1 The way A-WENO high-order correction terms are computed can be straightforwardly extended to the multidimensional case. They can also be extended to higher than fifth order of accuracy via high-order Taylor expansions; see, e.g., [19] for details on the seventh- and ninth-order A-WENO schemes.

3 Flux Globalization Based Well-Balanced Path-Conservative A-WENO Schemes for (1.2)

In this section, we extend the A-WENO schemes presented in §2 to the nonconservative systems (1.2) via a flux globalization based framework.

3.1 Flux Globalization Based A-WENO Schemes

We begin with the extension of A-WENO schemes to the nonconservative systems (1.2), written in the quasi-conservative form (1.3). A direct generalization of the semi-discrete A-WENO schemes (2.1)–(2.2) reads as

$$\frac{\mathrm{d}\boldsymbol{U}_j}{\mathrm{d}t}=-\frac{\boldsymbol{\mathcal{K}}_{j+\frac12}-\boldsymbol{\mathcal{K}}_{j-\frac12}}{\Delta x},\tag{3.1}$$

where $\boldsymbol{\mathcal{K}}_{j+\frac12}$ are the fifth-order numerical fluxes:

$$\boldsymbol{\mathcal{K}}_{j+\frac12}=\boldsymbol{\mathcal{K}}^{\rm FV}_{j+\frac12}-\frac{(\Delta x)^2}{24}(\boldsymbol{K}_{xx})_{j+\frac12}+\frac{7(\Delta x)^4}{5760}(\boldsymbol{K}_{xxxx})_{j+\frac12}.$$

Here, $\boldsymbol{\mathcal{K}}^{\rm FV}_{j+\frac12}=\boldsymbol{\mathcal{K}}^{\rm FV}_{j+\frac12}\big(\boldsymbol{U}^-_{j+\frac12},\boldsymbol{U}^+_{j+\frac12}\big)$ stand for FV numerical fluxes and in this paper, we use the central (local Lax-Friedrichs, Rusanov) fluxes

$$\boldsymbol{\mathcal{K}}^{\rm FV}_{j+\frac12}=\frac{\boldsymbol{K}\big(\boldsymbol{U}^-_{j+\frac12}\big)+\boldsymbol{K}\big(\boldsymbol{U}^+_{j+\frac12}\big)}{2}-\frac{a_{j+\frac12}}{2}\big(\boldsymbol{U}^+_{j+\frac12}-\boldsymbol{U}^-_{j+\frac12}\big)\tag{3.2}$$

with the local speeds of propagation estimated using the eigenvalues $\lambda_1(\mathcal{A})\le\ldots\le\lambda_d(\mathcal{A})$ of the matrix $\mathcal{A}=\frac{\partial\boldsymbol{F}}{\partial\boldsymbol{U}}(\boldsymbol{U})-B(\boldsymbol{U})$:

$$a_{j+\frac12}=\max_j\Big\{\big|\lambda_1\big(\mathcal{A}(\boldsymbol{U}^-_{j+\frac12})\big)\big|,\,\big|\lambda_1\big(\mathcal{A}(\boldsymbol{U}^+_{j+\frac12})\big)\big|,\,\big|\lambda_d\big(\mathcal{A}(\boldsymbol{U}^-_{j+\frac12})\big)\big|,\,\big|\lambda_d\big(\mathcal{A}(\boldsymbol{U}^+_{j+\frac12})\big)\big|\Big\}.$$

The global fluxes $\boldsymbol{K}^{\pm}_{j+\frac12}=\boldsymbol{K}(\boldsymbol{U}^{\pm}_{j+\frac12})$ in (3.2) are to be computed in such a way to ensure both WB and path-conservative properties of the resulting scheme. To this end, we follow the approach introduced in [26]. We first note that (1.2) admits steady-state solutions satisfying

$$\boldsymbol{F}(\boldsymbol{U})_x-B(\boldsymbol{U})\boldsymbol{U}_x=\boldsymbol{0}.\tag{3.3}$$

As it was shown in [26] (also see [3,4,10]), for many particular nonconservative systems the relation (3.3) can be written as

$$\boldsymbol{F}(\boldsymbol{U})_x - B(\boldsymbol{U})\boldsymbol{U}_x = M(\boldsymbol{U})\boldsymbol{E}(\boldsymbol{U})_x = \boldsymbol{0}, \tag{3.4}$$

where $M \in \mathbb{R}^{d\times d}$ and $\boldsymbol{E}$ is the vector of equilibrium variables. If M is invertible (which is the case in many practically interesting cases), the steady states satisfy the relation

$$\boldsymbol{E}(\boldsymbol{U}) \equiv \textbf{Const}.$$

Taking this into account, we evaluate $\boldsymbol{K}^{\pm}_{j+\frac{1}{2}}$ as follows:

$$\boldsymbol{K}^{\pm}_{j+\frac{1}{2}} = \boldsymbol{F}^{\pm}_{j+\frac{1}{2}} - \boldsymbol{R}^{\pm}_{j+\frac{1}{2}}, \tag{3.5}$$

where $\boldsymbol{F}^{\pm}_{j+\frac{1}{2}} := \boldsymbol{F}(\boldsymbol{U}^{\pm}_{j+\frac{1}{2}})$, and the point values $\boldsymbol{U}^{\pm}_{j+\frac{1}{2}}$ are to be obtained using a reconstruction of the equilibrium variables $\boldsymbol{E}$ to ensure the WB property. To this end, we first compute the point values $\boldsymbol{E}_j := \boldsymbol{E}(\boldsymbol{U}_j)$ and then apply the WENO-Z interpolation to evaluate $\boldsymbol{E}^{\pm}_{j+\frac{1}{2}}$. The corresponding values $\boldsymbol{U}^{\pm}_{j+\frac{1}{2}}$ are then computed by solving the (nonlinear systems of) equations

$$\boldsymbol{E}(\boldsymbol{U}^{+}_{j+\frac{1}{2}}) = \boldsymbol{E}^{+}_{j+\frac{1}{2}} \quad \text{and} \quad \boldsymbol{E}(\boldsymbol{U}^{-}_{j+\frac{1}{2}}) = \boldsymbol{E}^{-}_{j+\frac{1}{2}}$$

for $\boldsymbol{U}^{+}_{j+\frac{1}{2}}$ and $\boldsymbol{U}^{-}_{j+\frac{1}{2}}$, respectively. The point values of the global variable $\boldsymbol{R}^{\pm}_{j+\frac{1}{2}}$ in (3.5) are computed in a path-conservative way. We first select $\widehat{x} = x_{\frac{1}{2}}$, set $\boldsymbol{R}^{-}_{\frac{1}{2}} := \boldsymbol{0}$, evaluate

$$\boldsymbol{R}^{+}_{\frac{1}{2}} = \boldsymbol{B}_{\boldsymbol{\Psi},\frac{1}{2}}, \tag{3.6}$$

and then recursively obtain

$$\boldsymbol{R}^{-}_{j+\frac{1}{2}} = \boldsymbol{R}^{+}_{j-\frac{1}{2}} + \boldsymbol{B}_j, \quad \boldsymbol{R}^{+}_{j+\frac{1}{2}} = \boldsymbol{R}^{-}_{j+\frac{1}{2}} + \boldsymbol{B}_{\boldsymbol{\Psi},j+\frac{1}{2}}, \quad j = 1,\ldots,N_x. \tag{3.7}$$

In (3.6) and (3.7), $\boldsymbol{B}_j$ and $\boldsymbol{B}_{\boldsymbol{\Psi},j+\frac{1}{2}}$ are obtained using (3.4) and proper quadratures:

$$\begin{aligned}
\boldsymbol{B}_j &= \int\limits_{C_j} B\big(\boldsymbol{U}\big)\boldsymbol{U}_x\,\mathrm{d}x = \boldsymbol{F}^{-}_{j+\frac{1}{2}} - \boldsymbol{F}^{+}_{j-\frac{1}{2}} - \int\limits_{C_j} M\big(\boldsymbol{U}\big)\boldsymbol{E}(\boldsymbol{U})_x\,\mathrm{d}x,\\
\boldsymbol{B}_{\boldsymbol{\Psi},j+\frac{1}{2}} &= \int\limits_0^1 B\big(\boldsymbol{\Psi}_{j+\frac{1}{2}}(s)\big)\boldsymbol{\Psi}'_{j+\frac{1}{2}}(s)\,\mathrm{d}s\\
&= \boldsymbol{F}^{+}_{j+\frac{1}{2}} - \boldsymbol{F}^{-}_{j+\frac{1}{2}} - \frac{1}{2}\left[M\big(\boldsymbol{U}^{+}_{j+\frac{1}{2}}\big) + M\big(\boldsymbol{U}^{-}_{j+\frac{1}{2}}\big)\right]\big(\boldsymbol{E}^{+}_{j+\frac{1}{2}} - \boldsymbol{E}^{-}_{j+\frac{1}{2}}\big),
\end{aligned} \tag{3.8}$$

where $\boldsymbol{\Psi}_{j+\frac{1}{2}}(s) := \boldsymbol{\Psi}_{j+\frac{1}{2}}(s;\boldsymbol{U}^{-}_{j+\frac{1}{2}},\boldsymbol{U}^{+}_{j+\frac{1}{2}})$ is a sufficiently smooth path connecting the left- and right-sided states $\boldsymbol{U}^{-}_{j+\frac{1}{2}}$ and $\boldsymbol{U}^{+}_{j+\frac{1}{2}}$. We refer the readers to [15] for more details on the derivation of (3.8).

In order to ensure the designed flux globalization based WB path-conservative A-WENO scheme is fifth-order accurate, the integral $\boldsymbol{B}_j$ in (3.8) needs to be evaluated using at least a fifth-order quadrature. In this paper, we use the Newton-Cotes quadrature introduced in [13, (4.4)].

Finally, $(\boldsymbol{K}_{xx})_{j+\frac{1}{2}}$ and $(\boldsymbol{K}_{xxxx})_{j+\frac{1}{2}}$ are approximations of the second- and fourth-order spatial derivatives of $\boldsymbol{K}$ at $x = x_{j+\frac{1}{2}}$, which can be computed using the same FD approximations as in (2.3), namely, by

$$(\boldsymbol{K}_{xx})_{j+\frac{1}{2}} = \frac{1}{48(\Delta x)^2}\left(-5\boldsymbol{K}_{j-2} + 39\boldsymbol{K}_{j-1} - 34\boldsymbol{K}_j - 34\boldsymbol{K}_{j+1} + 39\boldsymbol{K}_{j+2} - 5\boldsymbol{K}_{j+3}\right),$$
$$(\boldsymbol{K}_{xxxx})_{j+\frac{1}{2}} = \frac{1}{2(\Delta x)^4}\left(\boldsymbol{K}_{j-2} - 3\boldsymbol{K}_{j-1} + 2\boldsymbol{K}_j + 2\boldsymbol{K}_{j+1} - 3\boldsymbol{K}_{j+2} + \boldsymbol{K}_{j+3}\right),$$

where $\boldsymbol{K}_j = \boldsymbol{F}(\boldsymbol{U}_j) - \boldsymbol{R}_j(\boldsymbol{U})$ and

$$\boldsymbol{R}_j(\boldsymbol{U}) = \int\limits_{\widehat{x}}^{x_j} B(\boldsymbol{U}(\xi,t))\boldsymbol{U}_\xi(\xi,t)\,\mathrm{d}\xi. \tag{3.9}$$

In order to obtain a fifth-order numerical scheme, the integral in (3.9) needs to be evaluated within the fifth order of accuracy. We refer to reader to, e.g., [12] for the fifth-order Newton-Cotes quadrature, which should be implemented in a recursive way.

3.2 More Efficient Flux Globalization Based A-WENO Schemes

In this section, we extend a new, more efficient A-WENO scheme from §2.2 to the nonconservative system (1.2). We now compute the high-order correction terms $(\boldsymbol{K}_{xx})_{j+\frac{1}{2}}$ and $(\boldsymbol{K}_{xxxx})_{j+\frac{1}{2}}$ with the help of the numerical fluxes:

$$(\boldsymbol{K}_{xx})_{j+\frac{1}{2}} = \frac{1}{12(\Delta x)^2}\Big[-\boldsymbol{\mathcal{K}}^{\mathrm{FV}}_{j-\frac{3}{2}} + 16\boldsymbol{\mathcal{K}}^{\mathrm{FV}}_{j-\frac{1}{2}} - 30\boldsymbol{\mathcal{K}}^{\mathrm{FV}}_{j+\frac{1}{2}} + 16\boldsymbol{\mathcal{K}}^{\mathrm{FV}}_{j+\frac{3}{2}} - \boldsymbol{\mathcal{K}}^{\mathrm{FV}}_{j+\frac{5}{2}}\Big],$$
$$(\boldsymbol{K}_{xxxx})_{j+\frac{1}{2}} = \frac{1}{(\Delta x)^4}\Big[\boldsymbol{\mathcal{K}}^{\mathrm{FV}}_{j-\frac{3}{2}} - 4\boldsymbol{\mathcal{K}}^{\mathrm{FV}}_{j-\frac{1}{2}} + 6\boldsymbol{\mathcal{K}}^{\mathrm{FV}}_{j+\frac{1}{2}} - 4\boldsymbol{\mathcal{K}}^{\mathrm{FV}}_{j+\frac{3}{2}} + \boldsymbol{\mathcal{K}}^{\mathrm{FV}}_{j+\frac{5}{2}}\Big].$$

Notice that here we do not need to evaluate the point values $\boldsymbol{K}_j$ and, in particular, we do not need to evaluate the integrals in (3.9). Therefore, the resulting new version of the flux globalization based WB path-conservative A-WENO scheme is substantially less computationally expensive than the scheme from §3.1.

Remark 3.1 As in the conservative case, the presented flux globalization based WB path-conservative A-WENO scheme can be straightforwardly extended to the multidimensional case and to higher than fifth order of accuracy via higher-order Taylor expansions.

4 Numerical Examples

For the sake of brevity, the A-WENO schemes from §2.1 and §3.1 will be referred to as the Old Schemes, while the A-WENO schemes from §2.2 and 3.2 will be referred to as the New Schemes. In this section, we will test the New and Old Schemes on six numerical examples.

We numerically integrate the ODE systems (2.1) and (3.1) by the three-stage third-order strong stability preserving (SSP) Runge-Kutta method (see, e.g., [20, 21]) and use the CFL number 0.45. In Example 4, where we test the accuracy of the studied A-WENO schemes, we take $\Delta t \sim (\Delta x)^{5/3}$ to ensure that the time errors do not dominate the spatial ones.

4.1 Scalar Equations

Example 1—Burgers Equation

In the first example, we consider the inviscid Burgers equation

$$u_t + \left(\frac{u^2}{2}\right)_x = 0$$

subject to the 1-periodic initial conditions

$$u(x,0) = \frac{1}{4} + \frac{1}{2}\sin(2\pi x).$$

We first compute the numerical solutions by both the New and Old Schemes on the uniform mesh with $\Delta x = 1/40$ in the computational domain $[0,1]$ until the final time $t = 0.4$. The obtained numerical results are plotted in Figure 4.1 along with the reference solution computed by the Old Scheme on a much finer mesh with $\Delta x = 1/2000$. As one can clearly see, the results obtained by the New and Old Schemes are almost identical.

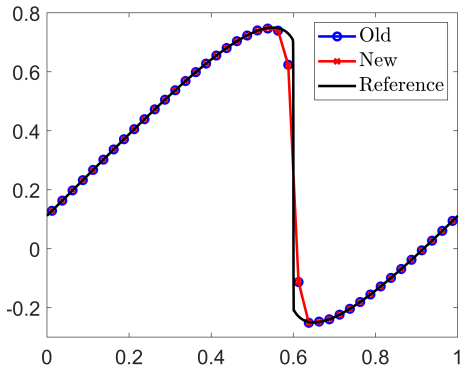

Figure 4.1: Example 1: Numerical solutions computed by the New and Old Schemes.

We then measure the CPU times consumed by both of the studied schemes and obtain that the CPU time consumed by the Old Scheme is about 4.5% larger than the CPU time consumed by the New Scheme. The difference is relatively small since the flux function $f(u) = u^2/2$ is very simple in this example.

Example 2—Buckley-Leverett Equation with Gravitational Effects

In the second example, we consider the Buckley-Leverett equation with gravitational effects, which reads as

$$u_t + \left[\frac{u^2}{u^2 + (1-u)^2}(1 - k(1-u)^2)\right]_x = 0.$$

We take $k = 1$, consider the 1-periodic initial conditions

$$u(x,0) = \frac{1}{4} + \frac{1}{2}\sin(2\pi x),$$

and compute the numerical solutions by both the New and Old Schemes on the uniform mesh with $\Delta x = 1/40$ in the computational domain $[0,1]$ until the final time $t = 0.4$. In Figure 4.2, we

present the obtained results along with the reference solution computed by the Old Scheme on a much finer mesh with $\Delta x = 1/2000$. As in Example 1, the New and Old solutions almost coincide. However, when we zoom at the area near the shock, one can see that the New Scheme produces less oscillatory solution than the Old Scheme.

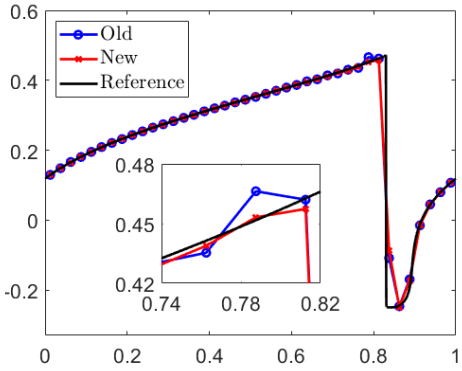

Figure 4.2: Example 2: Numerical solutions computed by the New and Old Schemes with the zoom at the left part of the shock area.

Next, we measure the CPU times consumed by both of the studied schemes and obtain that the CPU time consumed by the Old Scheme is about 7.2% larger than the CPU time consumed by the New Scheme. The efficiency gain is now bigger than in Example 1. This suggests that one can save more CPU time when the flux function is more complex.

Example 3—Scalar Equation with a Source Term

In the third example taken from [33], we consider the following nonconservative scalar equation:

$$u_t + f(u)_x + z_x u = 0, \quad f(u) = \frac{u^2}{2}, \quad z(x) = \begin{cases} -\cos(\pi x) & \text{if } x \in (\frac{3}{2}, \frac{5}{2}), \\ 0 & \text{otherwise.} \end{cases} \tag{4.1}$$

We take the constant initial datum $u(x,0) \equiv 1$ and impose the Dirichlet boundary conditions $u(0,t) = 2$ and $u(4,t) = 1$ on the interval $[0,4]$. It is easy to show that at the steady states $E := u + z \equiv \text{Const}$ and a scalar version of equation (3.4),

$$f(u)_x + z_x u = M(u)E_x = 0,$$

is satisfied with $M(u) = u$.

We follow §3 and design the Old and New Schemes for (4.1). We then compute the numerical solutions by both the obtained schemes on the uniform mesh with $\Delta x = 1/10$ until the final time $t = 2.75$ and present the snapshots of the computed solutions at $t = 0.25$, 0.75, 1.75, and 2.75 in Figure 4.3 along with the reference solution computed by the Old Scheme on a much finer mesh with $\Delta x = 1/10000$. Compared with the results reported in [33, §5], our solutions are sharper (as expected since our schemes are higher order). At the same time, one can clearly see that the results obtained by the New and Old Schemes are almost identical.

We then measure the CPU times consumed by both of the studied schemes and obtain that results show that the CPU times consumed by the Old Scheme are about 17.8% larger than the CPU time consumed by the New Scheme. The difference is larger than in Examples 1 and 2.

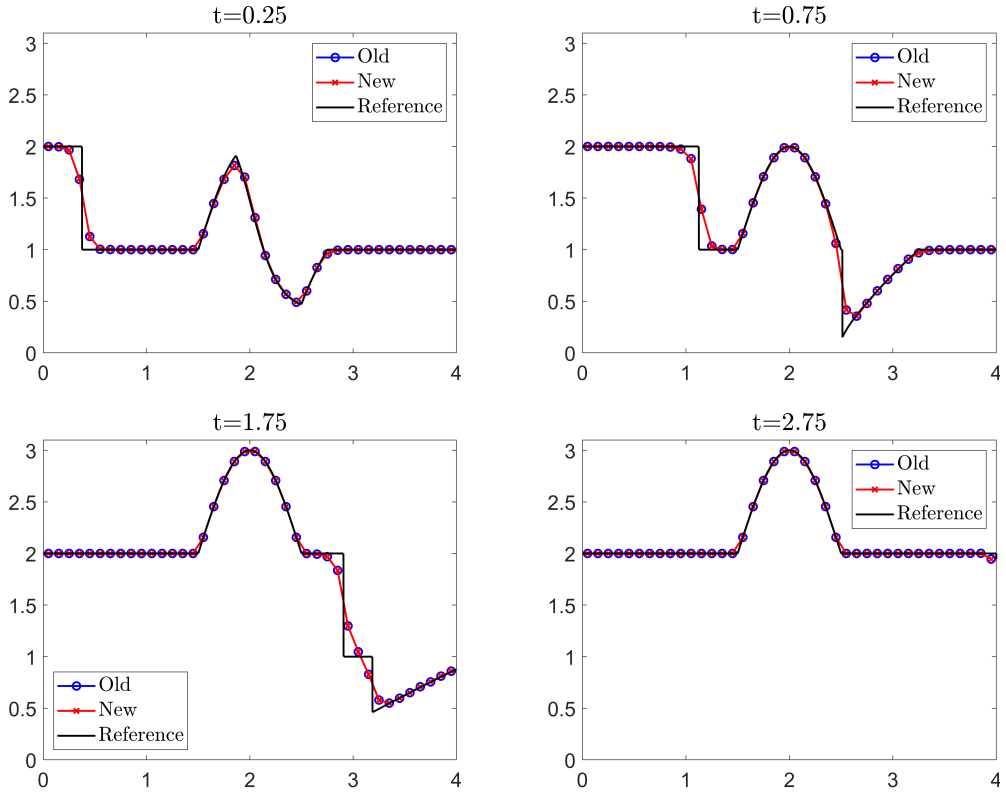

Figure 4.3: Example 3: Numerical solutions computed by the New and Old Schemes at different times.

This suggests that one can save much more CPU time by applying the new A-WENO schemes to nonconservative hyperbolic PDEs.

4.2 Euler Equations of Gas Dynamics

In this section, we consider the 1-D Euler equations of gas dynamics:

$$\rho_t + (\rho u)_x = 0, \tag{4.2}$$

$$(\rho u)_t + (\rho u^2 + p)_x = 0, \tag{4.3}$$

$$E_t + \big[u(E+p)\big]_x = 0, \tag{4.4}$$

where ρ, u, p, and E are the density, velocity, pressure and total energy, respectively. The system is completed through the equation of state for the ideal gas:

$$p = (\gamma - 1)\Big[E - \frac{1}{2}\rho u^2\Big], \tag{4.5}$$

where the parameter γ represents the specific heat ratio (we take $\gamma = 1.4$). When applying the studied A-WENO schemes to (4.2)–(4.5), we perform the WENO-Z interpolation in the local characteristic variables using the local characteristic decomposition, whose detailed description can be found in [11].

In Example 4, we test the accuracy of the New and Old Schemes and demonstrate that both the errors and experimental convergence rates are almost the same. In Examples 5 and 6, we consider more challenging numerical examples and demonstrate that the New Scheme is capable of achieving the same resolution as the Old Scheme.

Example 4—Accuracy Test

In this example taken from [25], we consider the following smooth initial data:

$$u(x,0)=\sin\Big(\frac{\pi x}{5}+\frac{\pi}{4}\Big),\quad \rho(x,0)=\left[\frac{\gamma-1}{2\sqrt{\gamma}}\,(u(x,0)+10)\right]^{\frac{2}{\gamma-1}},\quad p(x,0)=\rho^{\gamma}(x,0),$$

subject to the 10-periodic boundary conditions in the computational domain $[0,10]$.

We compute the numerical solutions by both the New and Old Schemes until the final time $t=0.1$ using both the New and Old Schemes on a sequence of uniform meshes with $\Delta x=1/20$, $1/40$, $1/80$, $1/160$, $1/320$, and $1/640$. The densities computed with $\Delta x=1/20$ are plotted in Figure 4.4 along with the reference solution computed by the Old Scheme on a much finer mesh with $\Delta x=1/320$, where one can clearly see that the results obtained by the New and Old Schemes are almost identical.

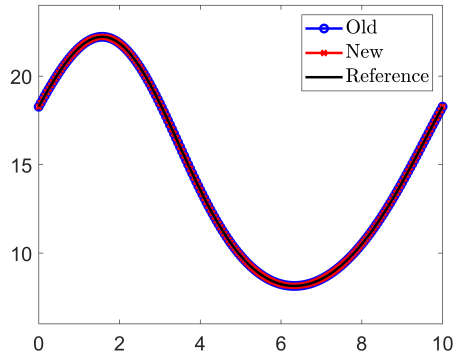

Figure 4.4: Example 4: Density ρ computed by the New and Old Schemes with $\Delta x=1/20$.

We then compute the L^1-errors and estimate the experimental convergence rates using the following Runge formulae, which are based on the solutions computed on the three consecutive uniform grids with the mesh sizes Δx, $2\Delta x$, and $4\Delta x$ and denoted by $(\cdot)^{\Delta x}$, $(\cdot)^{2\Delta x}$, and $(\cdot)^{4\Delta x}$, respectively:

$$\text{Error}(\Delta x)\approx\frac{\delta_{12}^2}{|\delta_{12}-\delta_{24}|},\quad \text{Rate}(\Delta x)\approx\log_2\left(\frac{\delta_{24}}{\delta_{12}}\right).$$

Here, $\delta_{12}:=\|(\cdot)^{\Delta x}-(\cdot)^{2\Delta x}\|_{L^1}$ and $\delta_{24}:=\|(\cdot)^{2\Delta x}-(\cdot)^{4\Delta x}\|_{L^1}$. The obtained results for the density and total energy are reported in Table 4.1, where one can clearly see that the fifth order of accuracy is achieved by the New Scheme and the errors are the same as those in the Old Scheme results.

Example 5—Shock Entropy Problem

In this example, we consider the shock-entropy problem introduced in [38]. The initial data are

$$(\rho,u,p)(x,0)=\begin{cases}(1.51695,0.523346,1.805), & x<-4.5,\\ (1+0.1\sin(20x),0,1), & x>-4.5.\end{cases}$$

We impose free boundary condition at the both ends of the computational domain $[-5,5]$ and compute the numerical solutions by both the New and Old Schemes until the final time $t=5$ on

Δx	New A-WENO Scheme				Old A-WENO Scheme			
	ρ		E		ρ		E	
	Error	Rate	Error	Rate	Error	Rate	Error	Rate
1/160	1.44e-09	4.79	2.13e-08	4.76	1.44e-09	4.79	2.13e-08	4.76
1/320	3.88e-11	5.00	5.65e-10	4.99	3.88e-11	5.00	5.65e-10	4.99
1/640	1.25e-12	4.98	1.81e-11	4.98	1.25e-12	4.98	1.81e-11	4.98

Table 4.1: Example 4: The L^1-errors and experimental convergence rates.

a uniform mesh with $\Delta x = 1/40$. The obtained numerical results are plotted in Figure 4.5 along with the reference solution computed by the Old Scheme on a much finer mesh with $\Delta x = 1/800$. As one can see from Figure 4.5 (right), where we zoom at the area where the solution has smooth oscillatory structures, the results obtained by the New and Old Schemes almost coincide, which suggests that the New Scheme is as accurate as the Old one.

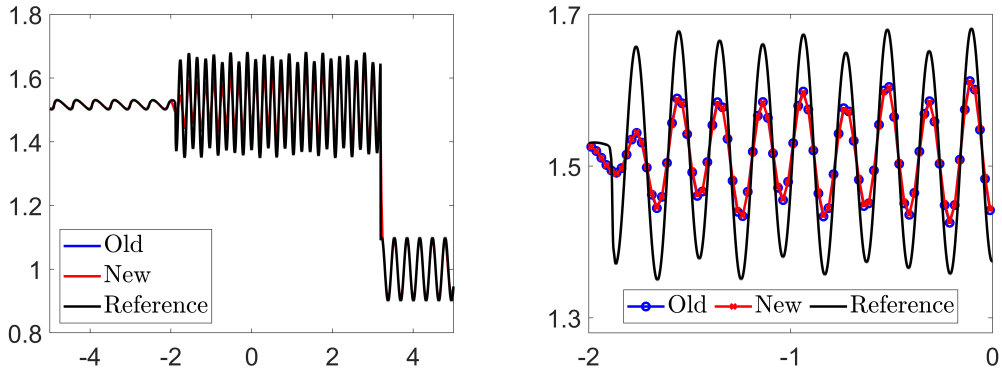

Figure 4.5: Example 5: Density computed by the New and Old Schemes (left) and zoom at $x \in [-2, 0]$ (right).

Example 6—Blast Wave Problem

In the last example taken from [43], we consider the following initial conditions:

$$(\rho, u, p)(x, 0) = \begin{cases} (1, 0, 1000), & x < 0.1, \\ (1, 0, 0.01), & 0.1 \le x \le 0.9, \\ (1, 0, 100), & x > 0.9, \end{cases}$$

subject to the solid wall boundary conditions imposed at the both ends of the computational domain $[0, 1]$.

We compute the numerical solutions until the final time $t = 0.038$ by both the New and Old Schemes on a uniform mesh with $\Delta x = 1/400$ and plot the obtained results in Figure 4.6 along with the reference solution computed by the Old Scheme on a much finer grid with $\Delta x = 1/8000$. Once again, one can see that the New and Old Schemes achieve the same resolution.

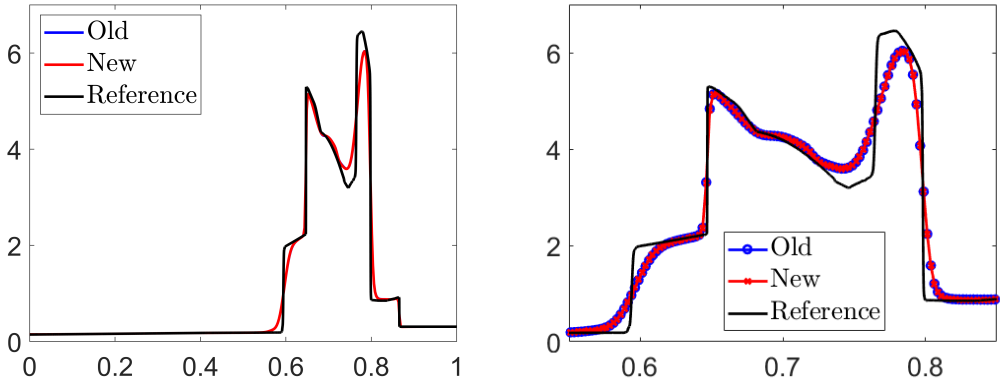

Figure 4.6: Example 6: Density computed by the New and Old Schemes (left) and zoom at $x \in [0.55, 0.85]$ (right).

5 Conclusions

In this paper, we have developed new more efficient fifth-order A-WENO schemes for both conservative and nonconservative nonlinear hyperbolic systems. A higher efficiency is achieved by utilizing the numerical fluxes in the computation of high-order correction terms. We have performed a careful numerical study of the proposed schemes and demonstrated that they may be up to 18% more efficient than the existing A-WENO schemes and at the same time, neither accuracy of capturing smooth parts of the solutions nor the resolution of discontinuous parts of the solution are affected by switching to the new approach.

Acknowledgment

The work of A. Kurganov was supported in part by NSFC grant 12171226 and by the fund of the Guangdong Provincial Key Laboratory of Computational Science and Material Design (No. 2019B030301001).

References

[1] R. Borges, M. Carmona, B. Costa, and W. S. Don, *An improved weighted essentially non-oscillatory scheme for hyperbolic conservation laws*, J. Comput. Phys., 227 (2008), pp. 3191–3211.

[2] S. Busto, M. Dumbser, S. Gavrilyuk, and K. Ivanova, *On thermodynamically compatible finite volume methods and path-conservative ADER discontinuous Galerkin schemes for turbulent shallow water flows*, J. Sci. Comput., 88 (2021). Paper No. 28, 45 pp.

[3] Y. Cao, A. Kurganov, Y. Liu, and R. Xin, *Flux globalization based well-balanced path-conservative central-upwind schemes for shallow water models*, J. Sci. Comput., 92 (2022). Paper No. 69, 31 pp.

[4] Y. Cao, A. Kurganov, Y. Liu, and V. Zeitlin, *Flux globalization based well-balanced path-conservative central-upwind scheme for two-layer thermal rotating shallow water equations*, J. Comput. Phys., 474 (2023). Paper No. 111790, 29 pp.

[5] M. Castro, B. Costa, and W. S. Don, *High order weighted essentially non-oscillatory WENO-Z schemes for hyperbolic conservation laws*, J. Comput. Phys., 230 (2011), pp. 1766–1792.

[6] M. J. Castro, T. Morales de Luna, and C. Parés, *Well-balanced schemes and path-conservative numerical methods*, in Handbook of numerical methods for hyperbolic problems, vol. 18 of Handb. Numer. Anal., Elsevier/North-Holland, Amsterdam, 2017, pp. 131–175.

[7] M. J. Castro and C. Parés, *Well-balanced high-order finite volume methods for systems of balance laws*, J. Sci. Comput., 82 (2020). Paper No. 48, 48 pp.

[8] M. J. Castro Díaz, A. Kurganov, and T. Morales de Luna, *Path-conservative central-upwind schemes for nonconservative hyperbolic systems*, ESAIM Math. Model. Numer. Anal., 53 (2019), pp. 959–985.

[9] C. Chalons, *Path-conservative in-cell discontinuous reconstruction schemes for non conservative hyperbolic systems*, Commun. Math. Sci., 18 (2020), pp. 1–30.

[10] Y. Chen, A. Kurganov, and M. Na, *A flux globalization based well-balanced path-conservative central-upwind scheme for the shallow water flows in channels*, ESAIM Math. Model. Numer. Anal., 57 (2023), pp. 1087–1110.

[11] A. Chertock, S. Chu, and A. Kurganov, *Adaptive high-order A-WENO schemes based on a new local smoothness indicator*, E. Asian. J. Appl. Math., 13 (2023), pp. 576–609.

[12] S. Chu, A. Kurganov, S. Mohammadian, and Z. Zheng, *Fifth-order A-WENO path-conservative central-upwind scheme for behavioral non-equilibrium traffic models*, Commun. Comput. Phys., 33 (2023), pp. 692–732.

[13] S. Chu, A. Kurganov, and M. Na, *Fifth-order A-WENO schemes based on the path-conservative central-upwind method*, J. Comput. Phys., 469 (2022). Paper No. 111508, 22 pp.

[14] S. Chu, A. Kurganov, and R. Xin, *A fifth-order A-WENO scheme based on the low-dissipation central-upwind fluxes*. To appear in the Proceedings of the XVIII International Conference on Hyperbolic Problems: Theory, Numerics, Applications.

[15] S. Chu, A. Kurganov, and R. Xin, *A Well-balanced fifth-order A-WENO schemes based on flux globalization*, submitted. Preprint available at ????

[16] G. Dal Maso, P. G. Lefloch, and F. Murat, *Definition and weak stability of nonconservative products*, J. Math. Pures Appl., 74 (1995), pp. 483–548.

[17] W. S. Don and R. Borges, *Accuracy of the weighted essentially non-oscillatory conservative finite difference schemes*, J. Comput. Phys., 250 (2013), pp. 347–372.

[18] W. S. Don, D.-M. Li, Z. Gao, and B.-S. Wang, *A characteristic-wise alternative WENO-Z finite difference scheme for solving the compressible multicomponent non-reactive flows in the overestimated quasi-conservative form*, J. Sci. Comput., 82 (2020). Paper No. 27, 24 pp.

[19] Z. Gao, L.-L. Fang, B.-S. Wang, Y. Wang, and W. S. Don, *Seventh and ninth orders alternative WENO finite difference schemes for hyperbolic conservation laws*, Comput. & Fluids, 202 (2020). Paper No. 104519, 17 pp.

[20] S. Gottlieb, D. Ketcheson, and C.-W. Shu, *Strong stability preserving Runge-Kutta and multistep time discretizations*, World Scientific Publishing Co. Pte. Ltd., Hackensack, NJ, 2011.

[21] S. Gottlieb, C.-W. Shu, and E. Tadmor, *Strong stability-preserving high-order time discretization methods*, SIAM Rev., 43 (2001), pp. 89–112.

[22] J. S. Hesthaven, *Numerical methods for conservation laws: From analysis to algorithms*, Comput. Sci. Eng. 18, SIAM, Philadelphia, 2018.

[23] Y. Jiang, C.-W. Shu, and M. P. Zhang, *An alternative formulation of finite difference weighted ENO schemes with Lax-Wendroff time discretization for conservation laws*, SIAM J. Sci. Comput., 35 (2013), pp. A1137–A1160.

[24] D. I. Ketcheson, R. J. LeVeque, and M. J. del Razo, *Riemann problems and Jupyter solutions*, vol. 16 of Fundamentals of Algorithms, SIAM, Philadelphia, PA, 2020.

[25] V. A. Kolotilov, A. A. Kurganov, V. V. Ostapenko, N. A. Khandeeva, and S. Chu, *On the accuracy of shock-capturing schemes calculating gas-dynamic shock waves*, Comp. Math. Math. Phys., 63 (2023), pp. 128–136.

[26] A. Kurganov, Y. Liu, and R. Xin, *Well-Balanced Path-Conservative Central-Upwind Schemes Based on Flux Globalization*, J. Comput. Phys., 474 (2023). Paper No. 111773, 32 pp.

[27] A. Kurganov and E. Tadmor, *New high-resolution semi-discrete central schemes for Hamilton-Jacobi equations*, J. Comput. Phys., 160 (2000), pp. 720–742.

[28] P. G. LeFloch, *Hyperbolic systems of conservation laws*, Lectures in Mathematics ETH Zürich, Birkhäuser Verlag, Basel, 2002. The theory of classical and nonclassical shock waves.

[29] P. G. Lefloch, *Graph solutions of nonlinear hyperbolic systems*, J. Hyperbolic Differ. Equ., 1 (2004), pp. 643–689.

[30] R. J. LeVeque, *Finite Volume Methods for Hyperbolic Problems*, Cambridge Texts in Appl. Math., Cambridge University Press, Cambridge, UK, 2002.

[31] H. Liu, *A numerical study of the performance of alternative weighted ENO methods based on various numerical fluxes for conservation law*, Appl. Math. Comput., 296 (2017), pp. 182–197.

[32] H. Liu and J. Qiu, *Finite difference Hermite WENO schemes for conservation laws, II: An alternative approach*, J. Sci. Comput., 66 (2016), pp. 598–624.

[33] M. Nolte and D. Kröner, *Well-balanced schemes for the initial boundary value problem for 1D scalar conservation laws*. Preprint available at https://arxiv.org/abs/math/0608567.

[34] C. Parés, *Path-conservative numerical methods for nonconservative hyperbolic systems*, vol. 24 of Quad. Mat., Dept. Math., Seconda Univ. Napoli, Caserta, 2009.

[35] E. Pimentel-García, M. J. Castro, C. Chalons, T. Morales de Luna, and C. Parés, *In-cell discontinuous reconstruction path-conservative methods for non conservative hyperbolic systems—second-order extension*, J. Comput. Phys., 459 (2022). Paper No. 111152, 35 pp.

[36] V. V. Rusanov, *The calculation of the interaction of non-stationary shock waves with barriers*, Ž. Vyčisl. Mat. i Mat. Fiz., 1 (1961), pp. 267–279.

[37] K. A. Schneider, J. M. Gallardo, D. S. Balsara, B. Nkonga, and C. Parés, *Multidimensional approximate Riemann solvers for hyperbolic nonconservative systems. Applications to shallow water systems*, J. Comput. Phys., 444 (2021). Paper No. 110547, 49 pp.

[38] C.-W. Shu and S. Osher, *Efficient implementation of essentially non-oscillatory shock-capturing schemes*, J. Comput. Phys., 77 (1988), pp. 439–471.

[39] E. F. Toro, *Riemann solvers and numerical methods for fluid dynamics: A practical introduction*, Springer-Verlag, Berlin, Heidelberg, third ed., 2009.

[40] B.-S. Wang, W. S. Don, N. K. Garg, and A. Kurganov, *Fifth-order A-WENO finite-difference schemes based on a new adaptive diffusion central numerical flux*, SIAM J. Sci. Comput., 42 (2020), pp. A3932–A3956.

[41] B.-S. Wang, W. S. Don, A. Kurganov, and Y. Liu, *Fifth-order A-WENO schemes based on the adaptive diffusion central-upwind Rankine-Hugoniot fluxes*, Commun. Appl. Math. Comput., 5 (2023), pp. 295–314.

[42] B.-S. Wang, P. Li, Z. Gao, and W. S. Don, *An improved fifth order alternative WENO-Z finite difference scheme for hyperbolic conservation laws*, J. Comput. Phys., 374 (2018), pp. 469–477.

[43] P. Woodward and P. Colella, *The numerical solution of two-dimensional fluid flow with strong shocks*, J. Comput. Phys., 54 (1988), pp. 115–173.